Thermal Dispersion and Convection Heat Transfer during Laminar Transient Flow in Porous Media

M.G. Pathak and S.M. Ghiaasiaan

GW Woodruff School of Mechanical Engineering
Georgia Institute of Technology, Atlanta, GA 30332

ABSTRACT

Solid-fluid thermal interactions during unsteady flow in porous media play an important role in the regenerators of pulse tube cryocoolers. Pore-level thermal processes in porous media under unsteady flow conditions are poorly understood. The objective of this investigation was to study the pore-level thermal phenomena during pulsating and unidirectional sinusoidal flow through a generic, two-dimensional porous medium by numerical analysis. Furthermore, an examination of the effects of flow pulsations on the thermal dispersion and heat transfer coefficient that are encountered in the standard, volume-average energy equations for porous media were carried out. Pulsating and unidirectional sinusoidal inlet flow rates were chosen as an intermediate step towards the more difficult problem of periodic flow. The investigated porous media are periodic arrays of square cylinders. Detailed numerical data for the porosities of 0.75 and 0.84, with flow pulsation frequencies of 0 - 80 Hz, were obtained at Reynolds numbers of 560 and 980. Based on these numerical data, the instantaneous as well as cycle-average thermal dispersion and heat transfer coefficients, to be used in the standard unsteady volume-average energy conservation equations for flow in porous media, were derived.

INTRODUCTION

The regenerator is among the most important components of Stirling and pulse-tube cryocooler systems. Regenerator systems within pulse-tube cryocoolers are generally made of porous filler structures, in most cases stacks of mesh metal or rare earth screens, and are therefore often modeled as porous media. The flow field in the aforementioned cryocooler cycles is periodic and therefore highly transient, however, rendering the applicability of the well-accepted analytical methods related to quasi-steady flow in porous media questionable. Pore-level thermal processes in porous media under unsteady flow are complicated. There are theoretical difficulties with respect to the applicability of the standard volume-average porous media formulation to fast transients. Furthermore, these standard volume-average equations can only be applied as semi-empirical postulated transport equations. The solid-fluid interactions, particularly frictional losses and thermal non-equilibria, in these porous structures strongly affect the overall performance of the cryocooler system [1]. Therefore, it is important to study the regenerator at the fundamental level (pore-level) in order to improve the understanding of regeneration in cryocooler cycles.

The study reported here follows our past experimental investigations and numerical simulations of PTR cryocoolers. Cha et al. [2] and Clearman et al. [3] performed experimental investiga-

Cryocoolers 16, edited by S.D. Miller and R.G. Ross, Jr.

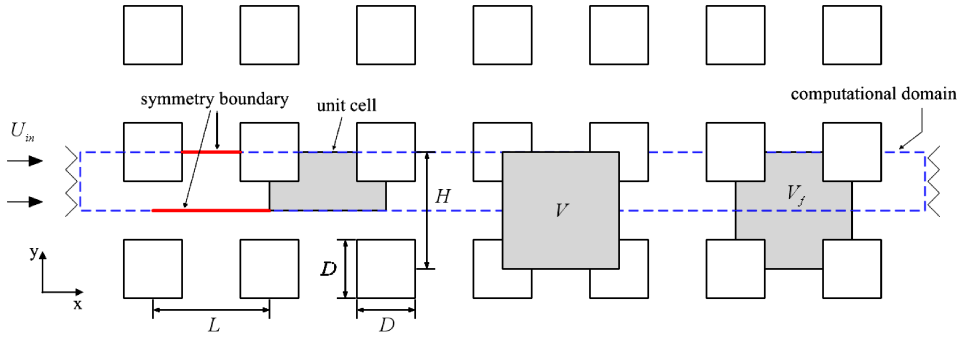

Figure 1. The simulated system.

tions of periodic flow in microporous media that are representative of the flow of cryogens in the regenerators of Stirling and pulse-tube cryocoolers. These studies have led to the development of empirical, cycle-average hydrodynamic closure relations suitable for volume-averaged conservation equations to be used for computational fluid dynamics (CFD) simulation of periodic flow in the porous components of cryocooler systems. The results have shown that the common practice of applying quasi-steady porous media model closure relations to transient flow conditions is far from reliable. Kim and Ghiaasiaan [4] demonstrated the feasibility of pore-scale numerical simulation of pulsating flow in micro porous structures using CFD tools equipped with specially-developed user defined functions (UDFs), with respect to the momentum transfer closure parameters.

The goal of this study is to investigate the pore-level flow and energy transport phenomena during transient flow through a microporous medium by direct numerical simulation using a CFD tool and UDFs. Fluent was used as the CFD tool, Gambit was used for CAD and mesh development, and C++ was used for UDF development.

SIMULATED SYSTEM

The simulated system for the numerical model will consist of two-dimensional arrays of rectangular cylinders, shown in Figure 1, following Kim and Ghiaasiaan [4].

The generic computational domain for this study is composed of six unit cells in series. The upper and lower surfaces of each unit cell consist of a symmetry boundary in order to optimize the computational processing efficiency. The square cylinders in this study were set to have an aspect ratio of $H/L = 1$, with H = 10 mm. The dimension D was parametrically changed in order to adjust the porosity. V and V_f represent the total volume and the volume the fluid occupied, respectively, in each unit cell. The porosity of the structure can be found from:

$$\varepsilon = 1 - \left(\frac{D}{L}\right)^2 \tag{1}$$

Previous studies performed by Kim [5] indicate that the end effects of the simulated row of the unit cells essentially disappear after the first few unit cells [5] with the addition of beginning and ending buffer zones and setting the inlet flow velocity to the entrance of the beginning buffer zone. This entire nodalized computational domain of the simulated system can be seen in Figure 2.

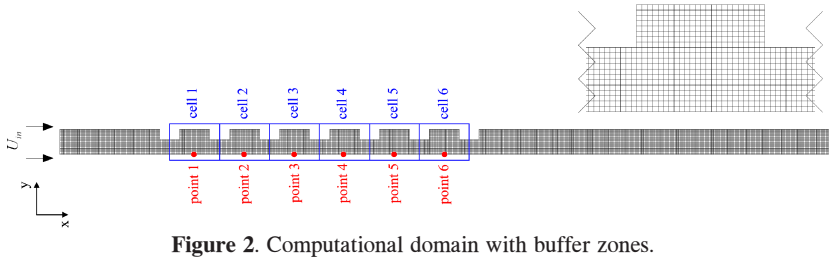

Figure 2. Computational domain with buffer zones.

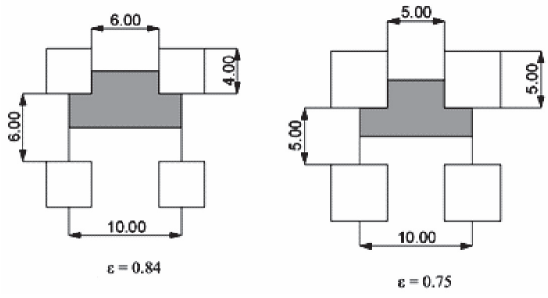

Figure 3. 75% and 84% porosity unit cell geometries.

The flow details in the fifth unit cell of the computational domain were thus investigated in order to eliminate the end effects in simulation. The unit cell geometries were altered according to Equation 1 so that porosities of 75% and 84% could be investigated. These geometrical details are shown in Figure 3.

The entire computational domain was meshed in Gambit with a 20×40 grid structure in order to ensure that convergence was achieved [5, 6].

THEORY

In modeling the flow and transport phenomena in porous media, volume averaged conservation equations are often used. Volume averaging is done over unit cells that represent the overall structure of the porous medium. For any local flow property, the instantaneous local property value can be separated into a fluid volume average term and a spatial deviation,

$$\phi = \langle \phi \rangle^f + \tilde{\phi} \tag{2}$$

where $\langle \phi \rangle^f = \frac{1}{V_f} \int_{V_f} \phi \, dV$ is the property term averaged over the fluid volume, and $\tilde{\phi}$ represents the spatial deviation from the volume averaged property. The fluid energy conservation equation can then be shown as [7],

$$\varepsilon \rho_f c_{pf} \left(\frac{\partial \langle T \rangle^f}{\partial t} + \frac{\partial}{\partial x_j} \langle u_j \rangle^f \langle T \rangle^f \right) = \frac{\partial}{\partial x_j} \left(\varepsilon k_f \frac{\partial \langle T \rangle^f}{\partial x_j} + \frac{k_f}{V} \int_{A_{int}} T n_j \, dA - \varepsilon \rho_f c_{pf} \left\langle \tilde{u}_j \tilde{T} \right\rangle^f \right) \tag{3}$$

Convection: $+\frac{1}{V} \int_{A_{int}} k_f \frac{\partial T}{\partial x_j} n_j \, dA$

Thermal Dispersion: $-\varepsilon \rho_f c_{pf} \left\langle \tilde{u}_j \tilde{T} \right\rangle^f$

The convection term in Equation 3 is often simplified by defining an interfacial heat transfer condition,

$$\frac{1}{V} \int_{A_{int}} k_f \frac{\partial T}{\partial x_j} n_j \, dA = a_f h_f \left(\langle T \rangle^s - \langle T \rangle^f \right) \tag{4}$$

The resulting energy equation can then be written,

$$\varepsilon \rho_f c_{pf} \left(\frac{\partial \langle T \rangle^f}{\partial t} + \frac{\partial}{\partial x_j} \langle u_j \rangle^f \langle T \rangle^f \right) = \frac{\partial}{\partial x_j} \left(\varepsilon k_f \frac{\partial \langle T \rangle^f}{\partial x_j} - \varepsilon \rho_f c_{pf} \left\langle \tilde{u}_j \tilde{T} \right\rangle^f \right) - a_f h_f \left(\langle T \rangle^f - \langle T \rangle^s \right) \tag{5}$$

The purpose of this investigation is to calculate and analyze the convection and thermal dispersion terms. This is done by directly solving the Navier-Stokes and energy conservation equations using very fine mesh structures in the system described in the previous section.

Two different Reynolds numbers can be defined, the pore – based Reynolds number [8] and the unit cell length – based Reynolds number [5], shown in Equations 6 and 7, respectively.

$$\mathrm{Re}_P = \frac{\rho_f \left|\left\langle \vec{u} \right\rangle\right| \sqrt{K}}{\mu_f} \tag{6}$$

$$\mathrm{Re}_L = \frac{\rho_f \left|\left\langle \vec{u} \right\rangle\right| L}{\mu_f} \tag{7}$$

In steady state, the flow remains laminar when $\mathrm{Re}_P < 300$. The simulations reported in this paper correspond to $\mathrm{Re}_L = 560$ and 980. The calculated Re_P values remained lower than 300. Therefore, the flow was assumed to remain in the laminar flow regime.

The inlet velocity to the system shown in Figure 2 was calculated from the following two equations.

$$U_{in} = U_m \left[1 + a \sin\left(2\pi f t\right)\right] \tag{8}$$

$$U_{in} = U_m \left|\sin\left(2\pi f t\right)\right| \tag{9}$$

where t represents time. Equation 8 evidently corresponds to pulsating flow. Equation 9, on the other hand, represents a pulsating flow in which an instant of a zero mean flow rate occurs in each cycle. This inlet condition will be referred to as unidirectional sinusoidal inlet flow, which is similar to periodic flow, without the complications of flow reversal. For pulsating flow, the amplitude a was set equal to 0.4. For both inlet flow types, the frequency, f, varied from 0 Hz to 80 Hz. These inlet velocities were imposed to the CFD simulations by developing specific UDFs.

Air, modeled as an incompressible fluid, was the working fluid. The temperature and pressure at inlet were assumed to be 200 K and 1 bar, respectively. The solid surfaces were assumed to remain at a temperature of 300 K. In the simulations, first the steady flow was simulated. The results were then used as the initial condition for the transient flow simulation. The transient simulations continued until steady periodic conditions were achieved. Fluent was used with pressure-based coupled algorithm to solve the mass, momentum, and energy conservation equations [9]. The simulation results were post processed in Matlab.

The instantaneous local temperature and velocity data were used to calculate the instantaneous volume average temperature and velocity, and these were in turn used for calculating the instantaneous local spatial temperature and velocity deviations. The instantaneous local spatial deviation of the temperature and velocity were then used for calculating the thermal dispersion and volume-averaged heat transfer coefficient. The resulting volume average convection coefficient was used for obtaining the volume-average cycle-average heat transfer coefficient.

To validate the heat transfer coefficient and thermal dispersion results, the volume average energy equation for flow in porous media, shown in Equation 5, was solved. The thermal dispersion and convection heat transfer terms obtained from direct simulations always satisfied the aforementioned differential equation.

RESULTS

The collected data presented in this section were obtained from the aforementioned pore-level, direct simulations. The volume and cycle average averaged (double-averaged) terms will be referred to as average terms for simplicity.

The resulting average convection heat transfer coefficients for the pulsating flow condition are plotted in Figure 4.

Figure 4 indicates that, for a given Reynolds number at a particular porosity, as the frequency increases, the average convection heat transfer coefficient monotonically increases. As expected the higher flow rates (larger Reynolds numbers) result in greater heat transfer coefficients. Also, it is noticed that the 84% porosity geometry has a lower heat transfer coefficient magnitude than the 75% porosity cases.

The average convection heat transfer coefficients obtained with the unidirectional sinusoidal inlet flow are shown in Figure 5. The trends are qualitatively similar to those for pulsating flow. The average convection coefficient increased as the frequency increased for a given flow rate at a par-

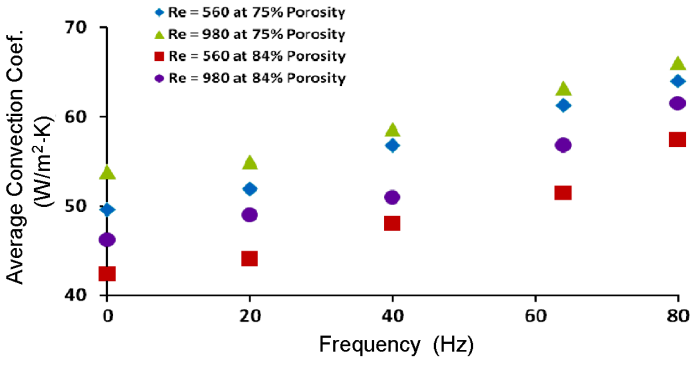

Figure 4. Average convection coefficient vs. frequency, pulsating flow.

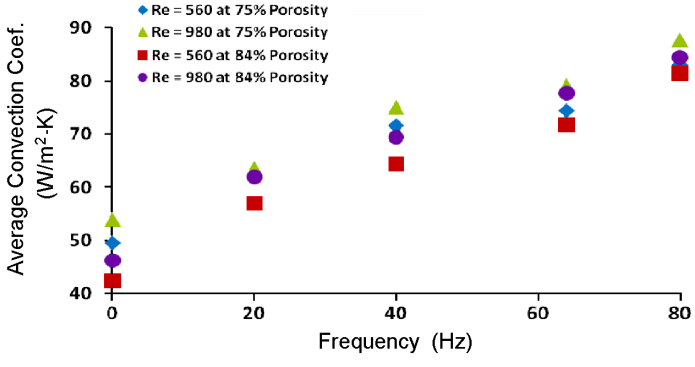

Figure 5. Average convection coefficient vs. frequency, unidirectional sinusoidal flow.

ticular porosity level, and increased with increasing Reynolds number. Also, the higher porosity configurations resulted in heat transfer coefficients that were lower in magnitude than the lower porosity geometries, consistent with the observations for the pulsating flow. Furthermore, the magnitude of the average convection heat transfer coefficients for unidirectional sinusoidal inlet flow is approximately 20% - 40% higher than the pulsating flow average convection heat transfer coefficients.

The average Nusselt number obtained from the pulsating flow condition is plotted against frequency in Figure 6, where the Nusselt number pertains to the unit cell length and is defined as,

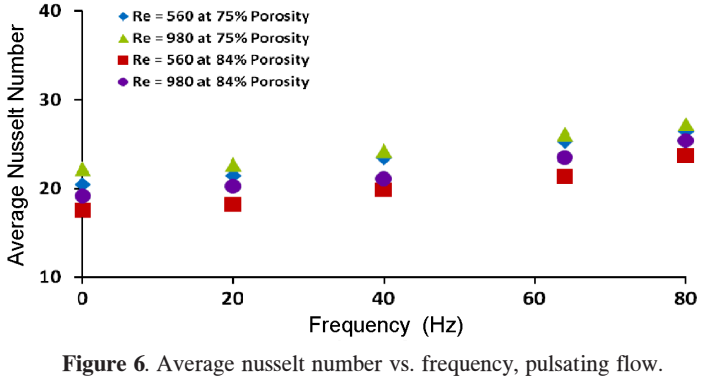

Figure 6. Average nusselt number vs. frequency, pulsating flow.

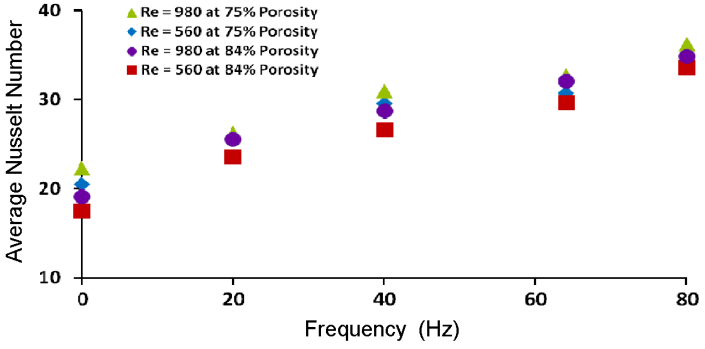

Figure 7. Average Nusselt number vs. frequency, unidirectional sinusoidal flow.

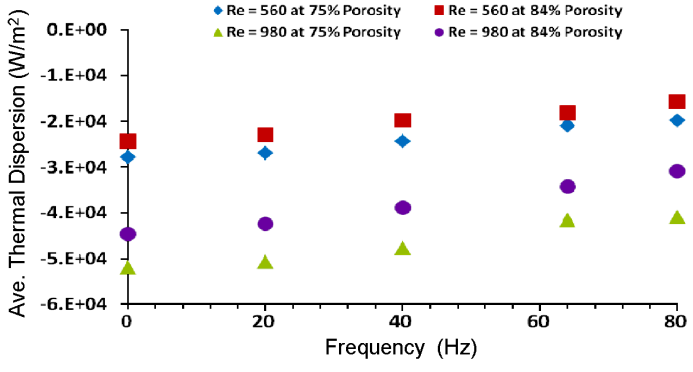

Figure 8. Average thermal dispersion vs. frequency, pulsating flow.

$$Nu_L = \frac{hL}{k_f} \tag{10}$$

Figure 7 displays the average Nusselt number extracted from the unidirectional sinusoidal inlet flow conditions. The trends in these two figures are similar to Figures 4 and 5, respectively, as expected.

The thermal dispersion term will now be discussed. The average thermal dispersion data for pulsating flow is presented in Figure 8. The thermal dispersion is defined as, $\varepsilon\rho_f c_{pf}\left\langle \tilde{u}_j\tilde{T}\right\rangle^f$. These results indicate that the thermal dispersion term increases with increasing frequency. It decreases as the Reynolds number is increased, and as the porosity is increased.

Figure 9 displays the average thermal dispersion data for the unidirectional sinusoidal inlet flow. The average thermal dispersion for the unidirectional sinusoidal inlet flow follows similar trends to that presented in the pulsating flow case. However, the unidirectional sinusoidal inlet flow average thermal dispersion values were greater than the pulsating flow configuration. Also, the pulsating flow data resemble a linear-like trendline whereas, the unidirectional sinusoidal flow case displays a more complicated trend.

The non-dimensional average thermal dispersion term, $\overline{\mathrm{TD}}$, defined in Equation 11, is plotted against frequency for the typical pulsating flow case in Figure 10.

$$\overline{\mathrm{TD}} = \frac{\varepsilon\rho_f c_{pf}\left\langle \tilde{u}_j\tilde{T}\right\rangle^f}{\rho c_p \varepsilon u_{\max} L\left(\left\langle \frac{dT}{dx}\right\rangle\right)} \tag{11}$$

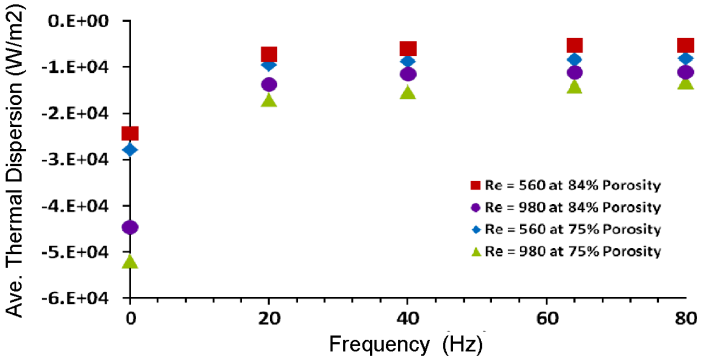

Figure 9. Average thermal dispersion vs. frequency, unidirectional sinusoidal flow.

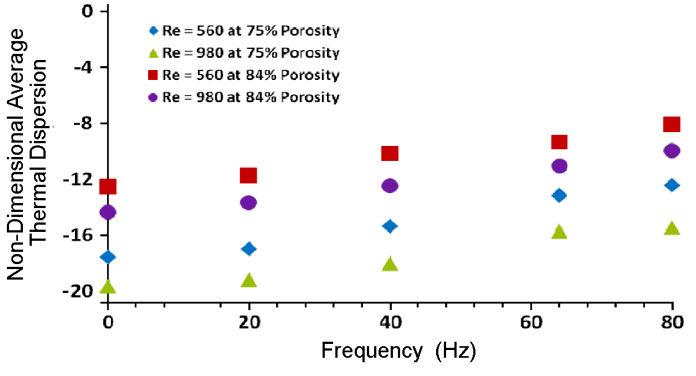

Figure 10. Non-dimensional average thermal dispersion vs. frequency, pulsating flow.

The non-dimensional term in Equation 11 compares the average thermal dispersion to the maximum change in the stored thermal energy in the fluid as it moved from one unit cell to another. The temperature gradient in this situation was found by applying the central differencing scheme in unit cell 5, using the temperature data from unit cell 4 and unit cell 6 in the simulated system.

The non-dimensional average thermal dispersion monotonically increased as the frequency increased. Similar to the average thermal dispersion trends show in Figure 8, $\overline{\mathrm{TD}}$ increased as the flow rate decreased, while holding the porosities constant, and $\overline{\mathrm{TD}}$ increased as porosity increased, while holding the flow rates fixed.

Figure 11 displays the non-dimensional average thermal dispersion term for the unidirectional sinusoidal inlet flow case. As expected, the collected data for $\overline{\mathrm{TD}}$ in Figure 11 show similar trends in comparison with the results presented in Figure 9. Also, it is noticed that the unidirectional sinusoidal inlet flow scenario results in the non-dimensional average thermal dispersion values to be greater than the values found for the pulsating flow condition.

The thermal dispersion in porous media is often modeled by defining a thermal dispersion conductivity tensor. Figures 12 displays the dependence of the instantaneous dimensionless dispersion thermal conductivity, k_{disp}/k_f, on the frequency for a typical set of parameters. The dispersion conductivity represents the axial direction of the simulated porous system. Figure 13 shows the insensitivity of the computed results to the number of nodes. The dispersion thermal conductivity in the axial direction is found from Equation 12.

$$k_{disp} = \frac{\varepsilon \rho_f c_{pf} \left\langle \tilde{u}_j \tilde{T} \right\rangle^f}{\varepsilon \left\langle \frac{dT}{dx} \right\rangle} \tag{12}$$

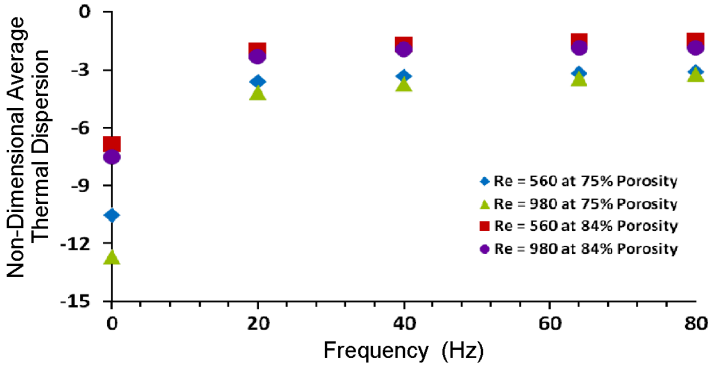

Figure 11. Non-dimensional average thermal dispersion vs. frequency, unidirectional sinusoidal flow.

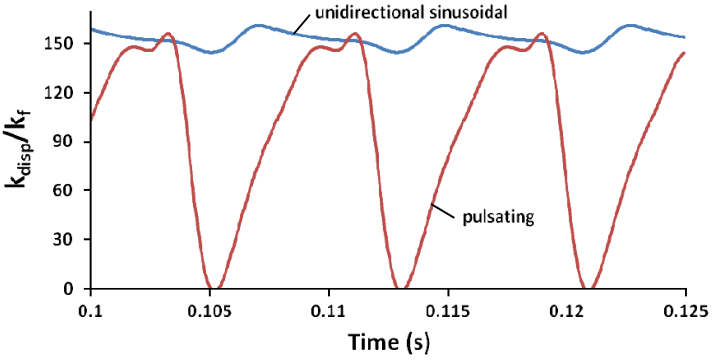

Figure 12. Variation of the axial thermal dispersion conductivity with frequency (Re_L = 980, ε=0.75).

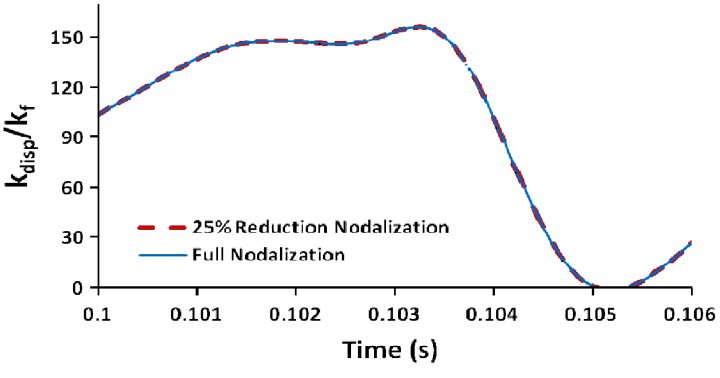

Figure 13. The effect of number of nodes on the thermal dispersion conductivity (Re_L = 980, ε=0.75).

Figure 12 shows that k_{disp} varies periodically during each cycle, and during a portion of each cycle it can be larger than the molecular thermal conductivity of the working fluid by orders of magnitude. Figures 12 and 13 also show the occurrence of a minor double periodicity. This type of double periodicity has been observed earlier [4], and is due to the re-circulatory patterns of the fluid that occur between the solid regions during each cycle.

CONCLUSION

In this study the solid-fluid heat transfer coefficients and the thermal dispersion effects were numerically investigated for a generic two-dimensional porous medium undergoing pulsating flow and unidirectional sinusoidal flow conditions. The numerical investigation was based on direct simulation of pore-level phenomena, and was carried out using Fluent CFD code. The generic porous media were formed by arrays of parallel square cylinders. The theoretical investigation revealed that both the average heat transfer coefficient and average thermal dispersion term increased with increasing frequency for a given Reynolds number (defined based on the unit cell characteristic dimension) at a particular porosity. The thermal dispersion was found to be typically orders of magnitude larger than the molecular conduction on the fluid. The instantaneous thermal dispersion conductivity in the axial direction was also calculated for typical simulation runs, and was found to vary periodically during each cycle.

Future plans include the calculation, assessment and possibly the correlation of the thermal dispersion and solid-fluid convection heat transfer coefficient for pulsating and unidirectional sinusoidal flows. We also plan to apply the knowledge gained from these results to tackle the more difficult problem of periodic flow in porous geometries representative of realistic cryocooler regenerators.

ACKNOWLEDGMENT

Special thanks are extended to Mr. Ted Conrad, a doctoral candidate in mechanical engineering at Georgia Institute of Technology, for his advice on using Fluent, developing UDF code, and guidance on parametric studies.

REFERENCES

1. Cha, J.S., Ghiaasiaan, S.M., Desai, P.V., Harvey, J.P., Kirkconnell, C.S., "Multi-Dimensional Effects in Pulse Tube Refrigerator," *Cryogenics* 46 (2006), pp. 658-665.
2. Cha, J.S., "Hydrodynamic Parameters of Microporous Media for Steady and Oscillatory Flow: Application to Cryocooler Regenerators," Doctoral Thesis, Georgia Institute of Technology, Atlanta, GA (2007).
3. Clearman, W.M., Cha, J.S., Ghiaasiaan, S.M., Kirkconnell, C.S., "Anisotropic Hydrodynamic Parameters of Microporous Media Applied in Pulse Tube and Stirling Cryocooler Regenerators," *Cryogenics* 48 (2008), pp. 112-121.
4. Kim, S.M., Ghiaasiaan, S.M., "Numerical Modeling of Laminar Pulsating Flow in Porous Media," *Journal of Fluids Engineering* 131 (2009).
5. Kim, S.M., "Numerical Investigation on Laminar Pulsating Flow Through Porous Media," Masters Thesis, Georgia Institute of Technology, Atlanta, GA (2008).
6. GAMBIT 2 User Manual, Fluent Inc., 2006.
7. Nakayama, A., Kuwahara, F., Kodama, Y., "An Equation for Thermal Dispersion Flux Transport and Its Mathematical Modeling for Heat Transfer and Fluid Flow in a Porous Medium," *Journal of Fluid Mechanics* 563 (2006), pp. 81–96.
8. de Lemos, M.J.S, & Pedras, M.H.J., "Recent mathematical models for turbulent flow in saturated rigid porous media," *Journal of Fluids Engineering* 123 (2001), pp. 935–940.
9. FLUENT 6.3 User Manual, Fluent Inc., 2008.